

# Vertical Motion of the Basin and Range, Western United States, from 10 Years of Campaign GPS

William C. Hammond  
Earthquake Hazards Team  
U.S. Geological Survey, Menlo Park, CA, 94025, United States

**Abstract.** An analysis of 10 years of campaign Global Positioning System (GPS) data collected in periodic surveys of the Basin and Range shows that vertical velocity measurement is less precise than horizontal measurements by approximately a factor of 3, and less precise than velocities from continuous GPS sites by a factor of 3-4. To obtain this level of precision, a method for conservatively quantifying uncertainties that takes into account the misfit of velocity data to a constant strain rate model is employed. This method results in a reduction of uncertainties by approximately a factor of 2. Uncertainties in position and velocity, for campaign and continuous sites are compared to results from other groups. Most of the vertical velocities in the Basin and Range are not resolvably different than zero, to 95% confidence. However, collecting sites into sub-networks of 10 sites indicates a marginally significant  $\sim 2$  mm/yr of vertical motion between  $114^\circ$  west longitude (up) compared  $119^\circ$  west longitude (down). The greatest east/west tilting rates are  $58.8 \pm 14.6$  nanoradians per year eastward and  $52.4 \pm 15.9$  nanoradians per year westward on the flanks of an area of relative uplift near  $114^\circ$  west longitude.

**Keywords.** Global Positioning System (GPS), vertical velocity, Basin and Range, western United States, extensional tectonics

---

## 1 Introduction

The Basin and Range province of the western United States is a region of active continental extension and transform deformation that accommodates relative motion between the Pacific, North American and Juan de Fuca plates. The name of the province comes from its pervasive topographic signature of north-south oriented ranges that form in response to normal fault controlled extension. The building of topographic relief represents a later stage of Basin and Range extension, ongoing since approximately 13 Ma (Zoback et al., 1981).

Recently, a number of space-based geodetic studies of contemporary Basin and Range deformation have

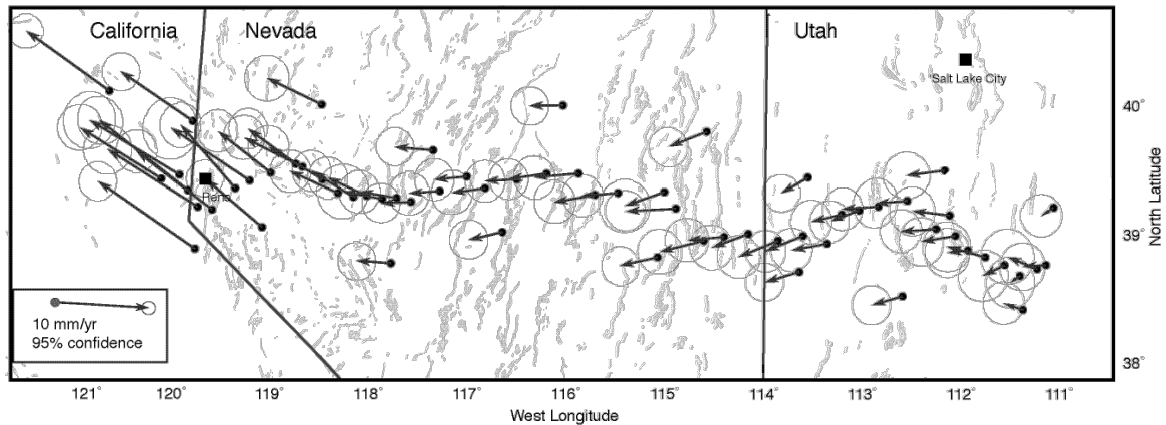
been undertaken (e.g. Thatcher et al., 1999; Oldow, 2000; Dixon et al., 2000; Wernicke et al., 2000; Miller et al., 2001; Svarc et al., 2002; Bennett et al., 2003), showing that nearly 25% of the  $\sim 50$  mm/yr relative horizontal motion between Pacific and North American plates occurs in the Basin and Range. Most of this relative motion is focused inside its westernmost 200 km, with approximately  $3.5 \pm 1.0$  mm/yr of it expressed as Pacific/North America relative plate motion normal extension.

Given the success of these studies, it is natural to examine the vertical motions that drive the formation of the spectacular relief in the Basin and Range. The presence of detectable ongoing extension suggests that vertical motions may also be detectable with the Global Positioning System (GPS). However, it is not clear what the expected magnitude of the vertical velocities will be. Vertical signals are expected from 1) broad-scale collapse of the province owing to gravitationally driven extension, 2) elastic strain accumulation on individual normal faults, 3) viscoelastic relaxation following historic earthquakes (e.g. Central Nevada Seismic Belt), and 4) non-tectonic signals such as those associated with volcanic centers, hydrological effects, and post-glacial isostatic rebound.

Beyond these complexities, the potential constraint that vertical motion offers on broad-scale continental geodynamics may be fundamental. If Basin and Range extension is driven by excess gravitational potential energy in the lithosphere, then vertical motions may be correlated with the inferred forces of gravity. Thus, learning more about long wavelength vertical motion will provide a new method for quantitative evaluation of the forces that drive western U.S. deformation.

The following is a description of how we estimate velocities and their uncertainties. Additionally, the Basin and Range campaign GPS dataset is used to evaluate the relative importance of different sources of uncertainty. I also present the vertical velocity results for our

Figure 1. GPS derived horizontal velocities for sites in the Basin and Range campaign GPS network. State lines are black. Faults active in Historic, Holocene or late Quaternary time are shown in light gray. Error ellipses show 95% confidence before uncertainty in the reference frame is estimated and removed.



Basin and Range campaign network and conclude that very little signal exists above the noise at this time. Further surveys will likely be required to reliably identify significant variation in vertical motion across the province.

## 2 Data

The Basin and Range network (Figure 1) consists of 90 geodetic benchmarks surveyed with campaign-GPS in 1992, 1996, 1998, and 2002. The 800 km long, roughly east-to-west line spans the entire province at approximately 39° north latitude, extending from east of the Wasatch Fault Zone in Utah (~111° west longitude) to west of the Genoa Fault Zone and Lake Tahoe (~120° west longitude) in the northern Sierra Nevada mountains of California. The network is identical to that described by Thatcher et al., (1999), except that 23 additional sites were added in 1998. Only 63 sites have sufficient data to derive velocities with reasonable uncertainties, and these are shown in Figure 1. Each site was visited with at least 4 years and at most 10 years between the first and most recent occupation. 55 sites have data spanning 10 years. Sites on the central east-west axis of the network (Figure 1) were generally observed twice for at least 6.5 hours per campaign, while the off-axis sites north and south of the main axis of the network were designed to be left unattended, and were occupied for between two and five 24 hour sessions per campaign. More information about this network and the data collected are provided in Hammond and Thatcher, 2003, submitted manuscript).

The daily positions of the stations were obtained by reducing the data with the GPS Inferred Position System/Orbit Analysis and Simulation (GIPSY/OASIS-II) software Linux version 2.6.1 (Webb and Zumberge, 1995), using the point

positioning method (Zumberge et al., 1997) and the final satellite and clock files from the Jet Propulsion Laboratory. Following point positioning, integer wavelength carrier phase ambiguities were estimated inside small, overlapping subsets of the stations, which reduced uncertainties. The site coordinates are effectively in a reference frame defined by the orbits of the satellites. Since we seek to understand motion in the western U.S., we transform the positions into a North America fixed reference frame. We transform the non-fiducial solutions into ITRF97 and then into a reference frame with minimum velocity for 13 continuously recording IGS stations presumed to represent rigid North America (ALGO, BRMU, CHUR, DRAO, GODE, KELY, MDO1, NLIB, RCM5, STJO, THU1, WES2, YELL, Prescott et al., 2001).

Once daily positions are obtained, constant velocities are estimated for each site through linear regression and a subsequent network adjustment using The Quasi-Observation Combination Analysis (QOCA, Dong et al., 1998) software. QOCA employs a Kalman filter to apply a daily Helmert transformation (7 total parameters for translation, rotation and scale) to insure that the inferred motions of all sites are as consistent as possible with velocities that are constant in time. Example time series for the off-axis site B300 and the on-axis site C260 are shown in Figure 2.

## 3 Uncertainties

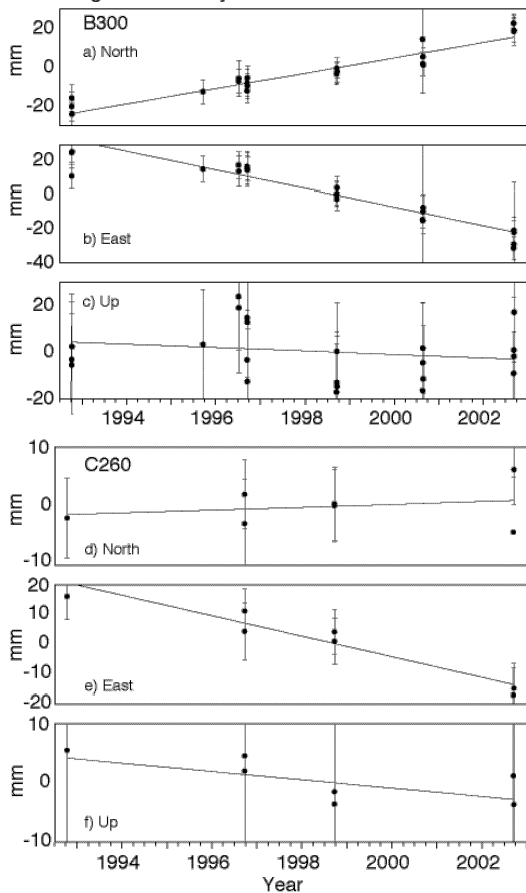
### 3.1 Estimation of Precision

Estimates of horizontal and vertical velocity are obtained in four steps. First, formal uncertainties in the individual positions are

obtained as output from the GIPSY/OASIS II software. The position uncertainties obtained in the 24 hour campaign sessions (Table 1) are similar to published studies (Eckl et al., 2001). They are also similar to results obtained from using BARGEN continuous site data (Bennett et al., 1998) when we used only data for the same days for which we had campaign data.

Second, we adjust the solution by applying the QOCA software to improve velocity estimation via removal of noise in the daily reference frame. This provides uncertainties that are on average more homogenous from site to site, and have correlation coefficients closer to zero than the un-adjusted velocities. Because we use point positioning, the covariance of velocities between adjacent sites is not retained and QOCA is unable to remove common mode uncertainty. Thus, the resulting

Figure 2. East, North and Up GPS time series for two stations B300 (off-axis) and C260 (on-axis). Error bars show 2 sigma uncertainty.



uncertainties in velocities with respect to the North America are greater than the uncertainties of velocities with respect to other sites in the network.

In the third step, the uncertainties in velocities are increased according to the estimated effects of time-correlated random walk noise (see e.g. Agnew,

1992; Langbein, 1997). We assume a constant value of  $1 \text{ mm/yr}^{1/2}$ , and add this as an uncorrelated component of the formal velocity uncertainty. The same value was used for the vertical and horizontal components.

Table 1. Comparison of campaign and continuous mode GPS mean daily position uncertainties.  $\sigma_N$ ,  $\sigma_E$ ,  $\sigma_U$  are one standard deviation formal uncertainty.

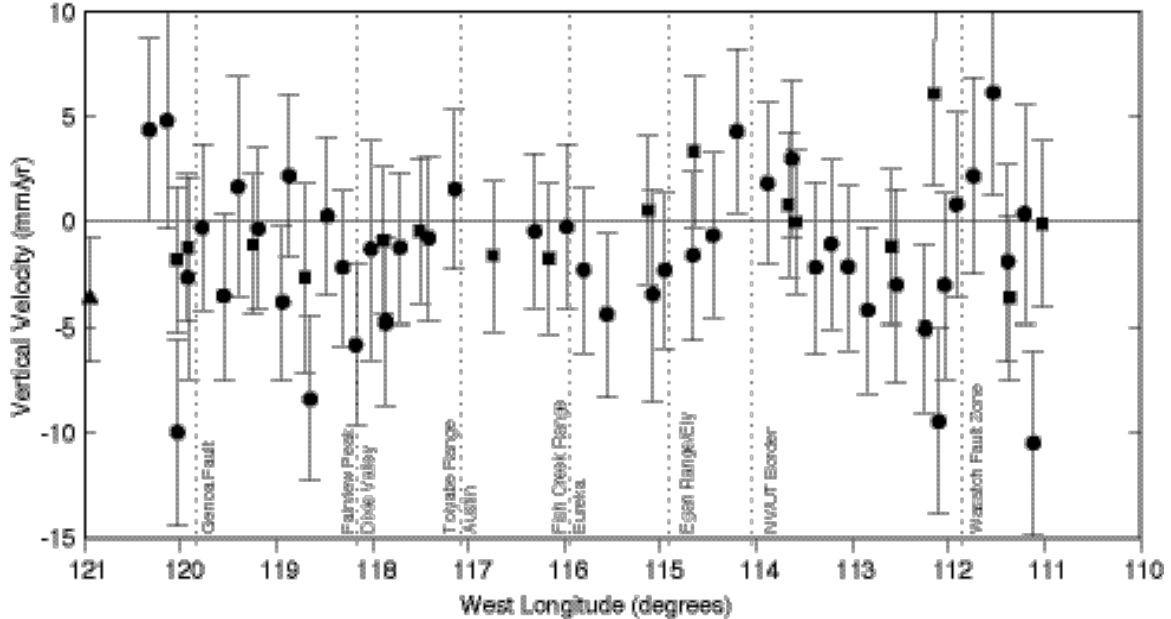
	$\sigma_N$	$\sigma_E$	$\sigma_U$
Campaign 6-8 hrs	6.8	7.3	22.1
Campaign 24 hrs	3.6	4.6	13.3
Continuous 24 hrs	3.5	5.4	13.3

In the fourth and final step, I reduce the uncertainties based on the observation that the variance of the velocities is significantly less than expected from the formal uncertainties. Misfit is summarized by

$$\chi^2 = \frac{1}{3N - M} (d - Gm)^T C_d^{-1} (d - Gm)$$

where  $N$  is the number of GPS sites,  $M=9$  is the number of parameters estimated in the inversion for the horizontal strain rate tensor (3 solid body translations and 3 rotations plus 3 strain rates),  $d$  is a vector of horizontal and vertical velocity components,  $C_d$  is a matrix whose diagonal contains the variances of velocity estimates, and  $Gm$  is the velocity predicted from the estimated constant strain rate tensor  $m$ . The strain rates are obtained using the spherical strain method of Savage et al., 2001, Appendix), and the evaluation of misfit is performed for many overlapping subsets of sites in the network. In the central Basin and Range the deformation rates are very low and a constant strain rate model fits the data very well (Davis et al., 2003; Hammond and Thatcher, 2003 submitted manuscript). Following step 3, the misfit  $\chi^2 \approx 0.2$ , suggests that we have overestimated the uncertainties. Thus, the uncertainties are scaled so that  $\chi^2 \approx 1.0$  inside the regions that have lowest misfit, i.e. in the central Basin and Range. The result is a scaling of the uncertainties by 0.44. When only vertical motions are analyzed the scaling is 0.54, indicating that horizontal and vertical uncertainties are similarly overestimated in steps 1-3. This procedure determines conservative (upper bound) uncertainty estimates since a more detailed strain rate model would tend to reduce uncertainties even more. Furthermore, this scaling is not sensitive to the type, or spectra, of the noise underlying the time series. The result is a realistic estimate of velocity uncertainty that preserves the relative variation in uncertainties obtained in steps 1-3.

Figure 3. Vertical velocity as a function of longitude across the Basin and Range. Error bars represent 95% confidence. Vertical dotted lines indicate features of interest.



The vertical velocities (Figure 3) have had this scale factor applied.

Because our primary interest is in deformation, we derive strain rates from the relative velocity between sites. However, because uncertainty exists in the reference frame determination, uncertainty in relative site velocity is smaller than uncertainty of velocity with respect to rigid North America. After step 3 above, reference frame uncertainty has been retained in each velocity estimate. However, after step 4 it has been mostly removed since we compare the velocities to a strain rate model. Consequently the scaling procedure of the previous paragraph is a proxy for removal of uncertainty in the reference frame, as is appropriate for deformation studies.

### 3.2 Campaign Mode GPS

Comparing measurements of uncertainty for different subsets of our data helps us understand the relative importance of the sources of noise in position and velocity uncertainty. I investigate the effects of benchmark type and quality, session length (in hours), and time interval between first and last observation (in years). Velocity uncertainties are summarized in Table 2. Because we are interested in deformation, we use the bracketed values from column A of Table 2, which have the misfit-based scaling applied.

The uncertainties in velocity are about 3-4 times those of the continuously recording BARGEN sites in the Basin and Range. Davis, et al., 2003) report

mean horizontal values of approximately 0.1 to 0.2 mm/yr, given approximately 6 years of continuous data (1996-2002), using a similar

Table 2. Mean campaign mode GPS velocity uncertainties ( $\sigma_{VN}$ ,  $\sigma_{VE}$ ,  $\sigma_{VU}$ ) in mm/yr and misfits ( $RMS_N$ ,  $RMS_E$ ,  $RMS_U$ ) in mm for the north, east, and up components respectively. Values in brackets are the most appropriate to use for tectonic deformation studies.

	A	B	C	D	E
$\sigma_{VN}$	0.86(0.76)[0.38]	0.92	0.54	0.76	0.90
$\sigma_{VE}$	1.02(0.92)[0.45]	1.08	0.66	0.90	1.11
$\sigma_{VU}$	2.85(2.86)[1.54]	3.26	1.66	2.60	2.69
$RMS_N$	4.16	4.07	4.45	4.25	2.54
$RMS_E$	4.71	4.52	5.32	4.79	3.81
$RMS_U$	16.26	14.84	20.84	16.7	7.72

A: All Campaign Sites with 1 mm/yr<sup>0.5</sup> random walk noise included, (in parenthesis random walk not included) [in brackets includes misfit-based scaling (see text)].

B: Same as A but just on-axis sites (6-8 hr sessions).

C: Same as A but just off-axis sites (24 hr sessions).

D: Same as A but just sites with >6 years of observation.

E: Same as A but just sites with <6 years of observation.

method as ours to scale the uncertainties. It may be surprising that our results are this precise, since the BARGEN monumentation is cross braced and deeply anchored, and their number of days of data is greater by about two orders of magnitude. However, the degradation of precision associated with re-occupation of a site with a campaign-style setup will likely affect RMS more than the formal uncertainty. Formal uncertainty is proportional to position uncertainty, which is nearly the same for continuous and 24 hour campaign sessions

Figure 4. a) Vertical velocity of subgroups of 10 sites across the Basin and Range with 95% confidence error bars, b) tilt rates around the horizontal north-south oriented axis for the same subgroups.

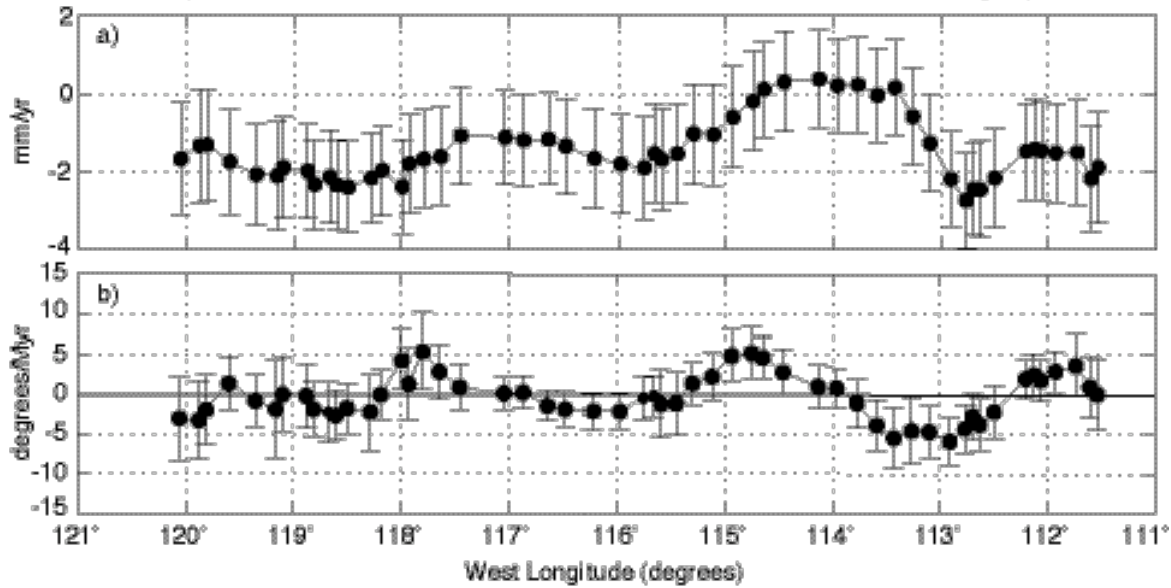


(Table 1), and is not affected by position scatter. For example, a line fit through a circular cloud of data may have the same formal uncertainty as a line fit through a nearly linear scatter, but their misfits (RMS) will differ greatly. Thus it is important to consider both measures of model quality. This can be seen in columns B and C in Table 2. 6-8 hour sessions have  $\sim 2$  times the uncertainty in position as 24 hour sessions, and thus formal uncertainty in velocity are about a factor of 2 greater. The effect of number of years ( $<6$  vs.  $>6$ , columns D & E of Table 2) is significant, but smaller than expected because the observations made in 1992 have greater uncertainty owing to fewer GPS satellites in the constellation and a weaker global ground-based tracking network. RMS is lower in column E because there are more sites where data was only collected in 1998 and 2002, making it relatively easy to fit a straight line.

#### 4 Vertical Velocity Results

The vertical velocities as a function of longitude are shown in Figure 3. They are not significantly (to 95% confidence) different from zero for 85% of the sites. In the few sites that have velocity significantly different than zero, there is no apparent long wavelength trend. On the westernmost and easternmost ends of the network the scatter of velocities suggests that most of what is seen is random variation. However, near 114° west longitude there is a local maximum vertical velocity, with flanks that extend between 116° and 112° west longitude. Solving for the tilt rates on horizontal axes oriented north-south and east-west

inside all contiguous sub-networks of 10 sites indicates that the east-west directed tilts are significant only on these flanks (Figure 4). Vertical velocity inside the same sub-networks shows that velocity variation across the network is marginally significant when comparing motion at 114° west to the lowest vertical velocity near 119°. Essentially, Figure 4a is a spatially smoothed view of Figure 3, and Figure 4b is the spatial derivative of Figure 4a. This feature is suggestive of the boudinage-like tilt domains discussed by Zuber, et al., (1986) that may form in response to rheological stratification of continental lithosphere.

#### 5 Conclusions

For 10 years of campaign GPS observations across the Basin and Range we have obtained vertical velocity uncertainties that average  $\sim 1.5$  mm/yr (1 standard deviation). This is approximately 3 times that of the horizontal components, and about 3-4 times vertical velocity uncertainty obtained by the BARGEN continuous network.

A small, marginally significant long wavelength uplift compared to the west end of the network may be detected near 114° west longitude. Maximum tilt rates of  $58.8 \pm 14.6$  nanoradians per year eastward and  $52.4 \pm 15.9$  nanoradians per year westward on its flanks are consistent with this uplift.

## 6 Acknowledgements

I would like to thank the ECGS and UNAVCO Inc. for hosting the “State of Vertical Positioning Precision” workshop and for their generous support that made my participation possible.

## References

- Agnew, D.C. (1992). The Time-Domain Behavior of Power Law Noises. *Geophys. Res. Lett.*, 19, 4, 333-336.
- Bennett, R.A., B.P. Wernicke and J.L. Davis (1998). Continuous GPS Measurements of Contemporary Deformation across the Northern Basin and Range Province. *Geophys. Res. Lett.*, 25, 4, 563-566.
- Bennett, R.A., B.P. Wernicke, N.A. Niemi, A.M. Friedrich and J.L. Davis (2003). Contemporary Strain Rates in the Northern Basin and Range Province from GPS Data. *Tectonics*, 22, 2, 3-1 - 3-31.
- Davis, J.L., R.A. Bennett and B.P. Wernicke (2003). Assessment of GPS Velocity Accuracy for the Basin and Range Geodetic Network (BARGEN). *Geophys. Res. Lett.*, 30, 7, 64-61 - 64-64.
- Dixon, T.H., M. Miller, F. Farina, H. Wang and D. Johnson (2000). Present-Day Motion of the Sierra Nevada Block and Some Tectonic Implications for the Basin and Range Province, North American Cordillera. *Tectonics*, 19, 1, 1-24.
- Dong, D., T.A. Herring and R.W. King (1998). Estimating Regional Deformation from a Combination of Space and Terrestrial Geodetic Data. *J. Geodesy*, 72, 200-214.
- Eckl, M.C., R.A. Snay, T. Soler, M.W. Cline and G.L. Mader (2001). Accuracy of GPS-Derived Relative Positions as a Function of Interstation Distance and Observing-Session Duration. *J. Geodesy*, 75, 633-640.
- Hammond, W.C. and W. Thatcher (2003). Contemporary Tectonic Deformation of the Basin and Range Province, Western United States: 10 Years of Observation with the Global Positioning System. *J. Geophys. Res.*, in preparation.
- Langbein, J. (1997). Correlated Errors in Geodetic Time Series; Implications for Time-Dependent Deformation. *J. Geophys. Res.*, 102, 1, 591-604.
- Miller, M.M., D.J. Johnson and T.H. Dixon (2001). Refined Kinematics of the Eastern California Shear Zone from GPS Observations, 1993-1998. *J. Geophys. Res.*, 106, 2, 2245-2263.
- Oldow, J.S. (2000). Tectonic Setting of the Central Walker Lane Transtensional Belt, Western Great Basin. *Abstracts with Programs - Geological Society of America*,
- Prescott, W.H., J.C. Savage, J.L. Svarc and D. Manaker (2001). Deformation across the Pacific-North America Plate Boundary near San Francisco, California. *J. Geophys. Res.*, 106, 4, 6673-6682.
- Savage, J.C., W. Gan and J.L. Svarc (2001). Strain Accumulation and Rotation in the Eastern California Shear Zone. *J. Geophys. Res.*, 106, 10, 21,995-922,007.
- Svarc, J.L., J.C. Savage, W.H. Prescott and A.R. Ramelli (2002). Strain Accumulation and Rotation in Western Nevada, 1993-2000. *J. Geophys. Res.*, 107, 5, 10.1029/2001JB000579.
- Thatcher, W., G.R. Foulger, B.R. Julian, J.L. Svarc, E. Quilty and G.W. Bawden (1999). Present-Day Deformation across the Basin and Range Province, Western United States. *Science*, 283, 1714-1718.
- Wernicke, B.P., A.M. Friedrich, N.A. Niemi, R.A. Bennett and J.L. Davis (2000). Dynamics of Plate Boundary Fault Systems from Basin and Range Geodetic Network (BARGEN) and Geologic Data. *GSA Today*, 10, 11, 1-7.
- Zoback, M.L., R.E. Anderson and G.A. Thompson (1981). Cainozoic Evolution of the State of Stress and Style of Tectonism of the Basin and Range Province of the Western United States. *Phil. Trans. Roy. Astron. Soc.*, 300, 407-434.
- Zuber, M.T., E.M. Parmentier and R.C. Fletcher (1986). Extension of Continental Lithosphere: A Model for Two Scales of Basin and Range Deformation. *J. Geophys. Res.*, 91, B5, 4826-4838.
- Zumberge, J.F., M.B. Heflin, D.C. Jefferson, M.M. Watkins and F.H. Webb (1997). Precise Point Positioning for the Efficient and Robust Analysis of GPS Data from Large Networks. *J. Geophys. Res.*, 102, 3, 5005-5017.